Two-Flux Radiation-Field Model for an Annular Packed-Bed Photocatalytic Oxidation Reactor

Gregory B. Raupp, Jill A. Nico, Suneetha Annangi, Rajnish Changrani, and Rao Annapragada
Dept. of Chemical, Bio & Materials Engineering, Arizona State University, Tempe, AZ 85287

One of the remaining challenges in application of heterogeneous photocatalysis for treatment of air streams containing dilute VOCs is to design a cost-effective photocatalytic reactor that simultaneously allows efficient contact of the contaminated air and solid catalyst while uniformly irradiating the solid catalyst with light. A pseudohomogeneous model was developed to study effects of system parameters on process performance for a gas–solid lamp-in-tube annular-photocatalytic-oxidation (PCO) reactor in which the annular space is filled with photocatalyst-coated packing. In this model the flow field is assumed to be uniform and radial diffusion negligible. Homogeneous reactions are neglected. Heterogeneous reaction rates follow Langmuir–Hinshelwood–Houghen–Watson kinetics with rate parameters extracted from independent experiments. A 1-D "two-flux" incidence submodel is used to account for the radial UV light distribution throughout the reactor annular space. This submodel requires knowledge of the UV lamp radiant emittance, the optical characteristics of the catalytic thin-film coating, and the UV irradiance at the outer wall of the reactor and contains only a single adjustable parameter — the mean free path between photon–catalyst interactions. The model was validated with experimental performance measurements for destruction of acetone and isopropyl alcohol in a bench-scale photoreactor. The validated model can be used to predict the optimum catalyst film thickness for given reactor dimensions, packing shape and size, and VOC abatement problem.

Introduction

Although there exists enormous potential for commercial application of gas–solid photocatalytic oxidation (PCO) to a wide variety of pollution remediation and control problems, a number of key unresolved technical issues must be addressed before this potential is fully realized. Perhaps the most significant unresolved issue is that of optimum photocatalytic reactor design. Although it is relatively straightforward to design a laboratory-scale reactor that simultaneously contacts a uniformly irradiated catalyst and air effectively (Formenti et al., 1971; Dibble and Raupp, 1990; Peral and Ollis, 1992), the issues of ultraviolet-light (UV) distribution and utilization (energy cost) make reactor design a difficult problem at the commercial level. The engineering science of heterogeneous *photo* catalytic-reactor design lags that for *thermal* catalytic-reactor design, largely because of the historical lack or scarcity of commercial applications for photocatalytic reactors.

In recent years, research groups at North Carolina State University (NCSU) and the National Renewable Energy Laboratory (NREL) have developed first-generation reactor models for several proposed PCO reactor configurations (Sauer, 1995; Wolfram, 1995). One prominent design, a lamp-in-tube annular reactor, features reasonably uniform irradiation of the titania photocatalyst coated on the inner wall of the outer tube. This "flow-by" design greatly simplifies modeling since a UV irradiation submodel is not required. However, in a commercial application, the design is not compact (low catalyst surface area to reactor volume ratio) and is susceptible to gas–solid diffusional mass-transport limitations. To enhance the active catalyst surface area to reactor volume ratio and to minimize diffusional limitations, many groups are now focusing on "flowthrough" designs, in which catalyst is distributed throughout the reactor volume. Example configurations include catalyst supported on a honeycombed monolith with external UV lamps (Suzuki, 1993), and catalyst supported on packing surrounding internal lamps.

Correspondence concerning this article should be addressed to G. B. Raupp.

In all photoreactors employing distributed catalysts, modeling is complicated by the distortions induced in the radiation field by the system heterogeneity. To our knowledge, a three-dimensional, rigorous radiation model for the source in combination with a first-principles scattering model has not been attempted. Instead, approximate one-dimensional solutions can be obtained with a two-flux model formulation (Akeheta et al., 1976; Inokawa and Akeheta, 1980; Maruyama and Nishimoto, 1992) or models employing light path-length distribution functions and light-dispersed phase-collision distribution functions (Yokota et al., 1977). Alternatively, two- and three-dimensional simulations can be obtained through Monte Carlo methods (Spadoni et al., 1978; Pasquali et al., 1996).

We have developed a base-case mathematical model to describe oxidation of a single contaminant in an air stream in a continuous packed-bed, lamp-in-tube photocatalytic reactor. A thin film of titania is coated on the exterior surface of the UV-transparent packing. The model accounts for simultaneous convection-diffusion and photocatalytic reaction in the presence of a radial gradient in UV irradiation predicted by a two-flux model. The two-flux submodel represents a trade-off between model complexity and accuracy of the prediction. This article describes the base-case model development and compares model predictions to experimental performance data.

Model Development

Overview

Figure 1 represents the physical reactor to be modeled. A feed stream of humid air containing a dilute concentration of volatile organic compounds (VOCs) flows between the solid packing in the reactor annular space. The cylindrical lamp emitting near UV light irradiates the surface of the titanium dioxide catalyst causing photocatalytic oxidation of the VOC to water and carbon dioxide. A gradient in UV intensity exists in the radial direction due to a simple geometric $1/r$ factor and due to the UV absorption and scattering by the photoactive thin film. This gradient will create a corresponding radial gradient in VOC reaction rate and in reactant and product concentrations.

The packing creates a complex three-dimensional flow pattern in the packed annular space that would be extremely difficult to model deterministically. A conventional approach in thermal catalytic reactor modeling for packed beds is to make a pseudohomogeneous simplification, in which the presence of a separate solid phase is not explicitly taken into account, and details of the flow hydrodynamics are not rigorously described (Froment and Bischoff, 1990). We adopt this approach in the current modeling effort.

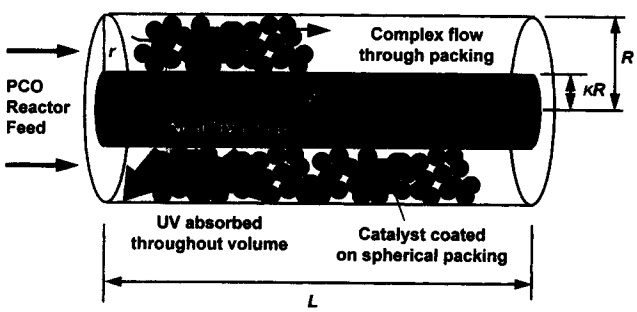

Figure 1. Physical model of the annular packed-bed reactor.

Based on the assumptions given below, the general equations for photoreactors can be reduced to i species mass balances, where i is the number of species in the overall reaction, and one UV radiation balance. The existence of the radial concentration gradient requires that two-dimensional species mass balances be employed. The species mass accounting statements and the radiation accounting statement are linked through the volumetric photocatalytic reaction-rate term in the species mass balances. However, because the reacting species do not absorb UV light, the radiation balance can be solved first, independently of the species balances. The resultant UV intensity profile from the two-flux UV irradiation submodel can then be used to solve the simultaneous pseudohomogeneous species mass-balance equations.

Pseudohomogeneous convection-reaction reactor model

The principal assumptions made in the development of the main reactor model consistent with the pseudohomogeneous framework are as follows:

- Steady-state operation
- Isothermal and isobaric conditions
- Axisymmetric
- Uniform effective catalyst density (uniform packing shape and distribution)
- Plug flow: fully developed axial uniform velocities for all z; negligible radial and angular velocities
- Axial dispersion present; negligible radial and angular effective diffusion
- Negligible radiant energy absorption by gaseous species
- Negligible thermal reactions
- Negligible heat of reaction (dilute reactants)
- Low and constant gas density

The axial dispersion contribution accounts for deviation from ideal plug flow. The light-intensity profile induces a radial VOC concentration gradient, and in physical reality radial diffusion will reduce the magnitude of the gradient. Neglecting radial diffusion is therefore a conservative assumption.

In packed reactors the support packing may not be distributed evenly about the axis, leading to departure from the axisymmetric assumption. In fact, it may be desirable to intentionally vary the size or shape of the packing in the radial direction in order to optimize the light distribution in the reactor space. Packing distribution is beyond the scope of this study, but ultimately could prove to be an important factor in heterogeneous photoreactor design.

Packing shape is another important factor in packed-reactor design. For most packed reactors the diffusion of the fluid species is dominated by the shape and packing distribution rather than the interaction of molecules. If $ReSc$ is greater than one, where Re is the Reynolds number and Sc is the Schmidt number, then support shape dominates effective diffusivities (Gunn, 1987). In order to utilize readily available data (Gunn, 1987) for the estimation of effective diffusivities, common simple packing shapes (i.e., solid spheres) were employed in model calculations.

The resulting species mass accounting statements for species i ($i = 1,2, \ldots$), Eq. 1, are second order in z and depend on r only in the reaction expression, since reaction rate is a function of the local rate of UV photon absorption by the solid catalyst:

$$\epsilon D_e \frac{d^2 c_i}{dz^2} - U_S \frac{dc_i}{dz} - \upsilon_i \Re = 0, \tag{1}$$

where
ϵ = reactor volume void fraction
D_e = effective axial diffusivity (area per unit time)
c_i = concentration of species i (mol per unit volume)
z = axial coordinate
U_S = superficial velocity (length per unit time)
υ_i = stoichiometric coefficient of species i
$\Re$ = overall reaction rate (mol per unit volume per unit time)

The superficial velocity is the hypothetical fluid plug-flow velocity that would be realized if the annular space was not packed, and is therefore given by

$$U_S = \frac{Q}{\pi r_0^2 (1 - \kappa^2)}, \tag{2}$$

where
Q = volumetric flow rate (volume per time)
r_0 = reactor outer-wall radius (length)
κ = ratio of UV lamp radius to reactor outer-wall radius (length per length)

It is assumed that the bulk species concentrations at the entrance to the reactor are known and that there is no concentration gradient at the reactor exit, yielding the following boundary conditions at the reactor inlet and outlet, respectively:

$$c_i|_{(z=0)} = c_{io} \tag{3}$$

$$\left.\frac{dc_i}{dz}\right|_{(z=L)} = 0, \tag{4}$$

where
c_{io} = inlet concentration (moles per unit volume)
L = reactor length (length)

UV radiation submodel

The UV radiation balance is an extension of the two-flux model of Maruyama and Nishimoto (1992). In the Maruyama and Nishimoto model, a one-dimensional irradiance balance was performed on a thin section of a *parallel-plate* reactor containing a low to moderate concentration of solid particles dispersed in a continuous transparent medium. The model accounted for light transmission past the particles, and reflection and absorption of light by the particles. Transmission *through* the particles was *not* considered.

The UV radiation submodel described in this article utilizes *cylindrical* coordinates and includes not only the effects of UV bypassing past the coated support particles and reflection by the catalyst film, but also partial absorption by *and transmission through* the absorbing catalyst layers. We make the following simplifying assumptions:

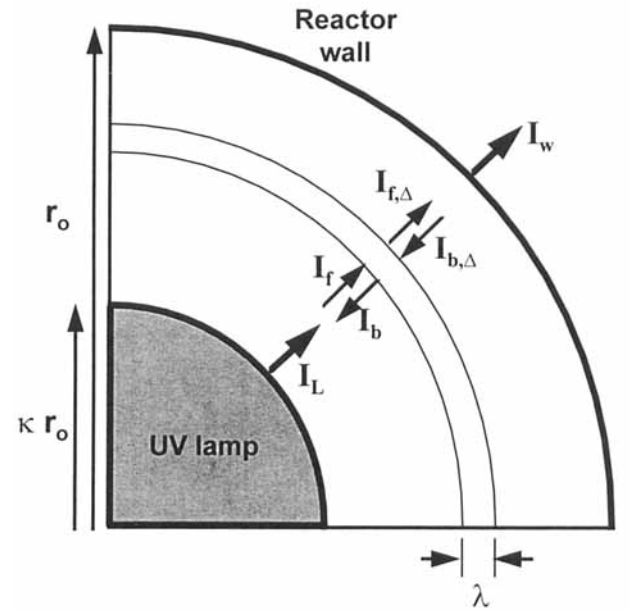

Figure 2. Two-flux model for the annular-reactor configuration.

- UV irradiance varies only in the radial direction (the model is 1-D).
- The total UV irradiance at a given point is the sum of the forward and backward irradiances (two-flux model).
- The continuous phase (air) is completely UV-transparent.
- The catalyst support is completely UV-transparent.
- The catalyst is coated uniformly on the packing.
- Catalyst support is distributed uniformly in the annular space.
- Catalyst support shape is uniform (e.g., identical diameter spheres).
- Film optical properties (reflectance R, absorbance A) are independent of wavelength.
- Reactor walls are made of nonabsorbing, nonreflecting material.

Figure 2 presents a physical picture of the two-flux model "shell" balance on a differential radial length λ chosen to be equal in magnitude to the photon mean free path. The resulting accounting statements for the forward UV flux I_f and the backward UV flux I_b are:

$$I_{f,\Delta} = (1 - C) \cdot I_f + C \cdot T \cdot I_f + C \cdot R \cdot I_{b,\Delta} \tag{5}$$

$$I_b = (1 - C) \cdot I_{b,\Delta} + C \cdot T \cdot I_{b,\Delta} + C \cdot R \cdot I_f, \tag{6}$$

where
$I_{f,\Delta}$ = forward irradiance at $r + \lambda$ (photons per unit area per unit time)
I_f = forward irradiance at r
$I_{b,\Delta}$ = backward irradiance at $r + \lambda$
I_b = backward irradiance at r
C = projected catalyst surface area per unit cross-sectional area
T = transmittance (fraction light transmitted)
R = reflectance (fraction light reflected)

The first terms on the righthand side of the irradiance balance Eqs. 5 and 6 represent the light that *bypasses* the sup-

port particles, and hence the catalyst film. The second terms represent the light that *transmits through* the supported catalyst film without being absorbed or reflected. The third terms represent the light that is *reflected* by the catalyst coating on the support particles.

For cylindrical symmetry, the UV flux varies with radial distance due to the increasing area for light dispersion with increasing distance from the light source. In terms of the variables defined previously:

$$I_{f,\Delta} = I_f + \lambda \frac{1}{r}\frac{d}{dr}(rI_f). \tag{7}$$

$$I_{b,\Delta} = I_b + \lambda \frac{1}{r}\frac{d}{dr}(rI_b). \tag{8}$$

These relationships are substituted into Eqs. 5 and 6, and the resulting equations are solved for the forward and backward UV photon-flux radial gradients to yield the governing two-flux model equations:

$$\frac{dI_f}{dr} = -\left\{\frac{1}{\lambda}\cdot\left[C(1-T)+\frac{(CR)^2}{1-C(1-T)}\right]+\frac{1}{r}\right\}\cdot I_f + \frac{1}{\lambda}\cdot\left\{\frac{CR}{1-C(1-T)}\right\}\cdot I_b \tag{9}$$

$$\frac{dI_b}{dr} = -\frac{1}{\lambda}\cdot\left\{\frac{CR}{1-C(1-T)}\right\}\cdot I_f + \left\{\frac{1}{\lambda}\cdot\left[\frac{C(1-T)}{1-C(1-T)}\right]-\frac{1}{r}\right\}\cdot I_b. \tag{10}$$

Knowledge of the forward flux, I_L, at the lamp surface and the forward flux, I_W, at the reactor outer-wall surface provide the boundary conditions necessary to solve the resulting radiation balance equations. Mathematically,

$$I_f|_{r=\kappa r_0} = I_L \tag{11}$$

$$I_f|_{r=r_0} = I_W, \tag{12}$$

where
I_L = irradiance at the lamp surface
I_W = irradiance at the reactor outer wall

One can use knowledge of the optical characteristics of the reactor outer wall to define an alternative boundary condition. For example, if the wall is nonreflecting, then the backward flux at the wall is zero and the following boundary condition applies:

$$I_b|_{r=r_0} = 0. \tag{13}$$

To more readily comprehend the effect of the magnitude on the various physical parameters of the system on the resulting UV flux profile, we define the dimensionless variables $\Theta \equiv I/I_L$ and $\xi \equiv r/r_0$, to create the following dimensionless version of Eqs. 9 through 12:

$$\frac{d\Theta_f}{d\xi} = -\left\{\left(\frac{r_0}{\lambda}\right)\cdot\left[C(1-T)+\frac{(CR)^2}{1-C(1-T)}\right]+\frac{1}{\xi}\right\}\cdot\Theta_f + \left\{\left(\frac{r_0}{\lambda}\right)\cdot\left[\frac{CR}{1-C(1-T)}\right]\right\}\cdot\Theta_b \tag{14}$$

$$\frac{d\Theta_b}{d\xi} = -\left\{\left(\frac{r_0}{\lambda}\right)\cdot\left[\frac{CR}{1-C(1-T)}\right]\right\}\cdot\Theta_f + \left\{\left(\frac{r_0}{\lambda}\right)\cdot\left[\frac{C(1-T)}{1-C(1-T)}\right]-\frac{1}{\xi}\right\}\cdot\Theta_b \tag{15}$$

$$\Theta_f|_{\xi=\kappa} = 1 \tag{16}$$

$$\Theta_f|_{\xi=1} = I_W/I_L. \tag{17}$$

Inspection of these equations reveals that the dimensionless (or normalized) UV flux profile is determined by the magnitudes of the following four dimensionless groups:

$$N_p = \frac{r_0}{\lambda} \tag{18}$$

$$N_f = C(1-T)+\frac{(CR)^2}{1-C(1-T)} \tag{19}$$

$$N_r = \frac{CR}{1-C(1-T)} \tag{20}$$

$$N_b = \frac{C(1-T)}{1-C(1-T)}. \tag{21}$$

The magnitudes of each of these respective groups depend on the physical dimensions of the annular reactor and packing size and/or the physical and optical nature of the supported catalyst film. Because the mean free path λ is directly related to the size and shape of the packing, the first dimensionless group, N_p, is a measure of the packing density. The greater the density, the greater the value of N_p, and consequently all coefficients in the differential equations Eqs. 14 and 15, leading to greater interaction between the UV light and the solid catalyst and a more severe UV flux gradient in the radial direction. The other three groups relate to the extent of UV light–catalyst interaction. The magnitudes depend on the optical constants of the catalyst film.

The factor $1-C\,(1-T)$ appearing in the denominators of the dimensionless groups defined in Eqs. 18 through 21 is the fraction of incident light that either bypasses the catalyst or is transmitted through the catalyst, which for purposes of brevity we will refer to as the fraction transmitted. The forward-interaction number, N_f, is then the sum of the fraction of incident forward light reflected or absorbed plus the ratio of the fraction of light double reflected over the fraction transmitted. The backward-interaction number, N_b, is the ratio of the fraction of incident light in the backward direction that is either reflected or absorbed to the fraction transmitted. The reflection number, N_r, is the ratio of the incident light reflected to the fraction transmitted. The greater the magnitude of these three groups, the greater the UV light–catalyst interaction, and hence the greater the UV flux gradient. The

greater the reflection number, the greater the contribution of the backward flux to the overall flux profile, and the greater the backward-reflection loss.

Constitutive relationships

Constitutive relations are needed to complete the model. A reaction-rate expression valid over the entire range of local conditions (reactant and product concentrations, UV flux) is crucial to accurate reactor-model predictions. In this work we adopt the following semiempirical Langmuir–Hinshelwood–Hougen–Watson (LHHW) kinetic rate form for the rate of reaction per gram of catalyst suggested by researchers at NREL (Turchi, 1995):

$$R = (\mathrm{LVREA}\cdot\Phi_{\mathrm{VOC}})\left\{\frac{K_{\mathrm{VOC}}C_{\mathrm{VOC}}}{1+K_{\mathrm{VOC}}C_{\mathrm{VOC}}+K_W C_W}\right\}, \quad (22)$$

where

LVREA = local volumetric rate of energy absorption (mole photons per unit time per unit volume)
Φ_{VOC} = mole VOC converted per mole photons absorbed
K_{VOC} = equilibrium adsorption constant for the VOC (volume per mol)
C_{VOC} = VOC concentration (mol VOC per unit volume)
K_W = equilibrium adsorption constant for water vapor (volume per mol)
C_W = water vapor concentration (mol water vapor per unit volume)

The first term in parentheses lumps the complex photocatalytic initiation steps together. The LVREA is determined from a local UV intensity balance using the solution of the two-flux submodel. The second term in brackets represents the fraction of the catalyst surface sites that are covered by adsorbed VOC. The $K_W C_W$ term in the denominator accounts for the typically observed inhibition of the photocatalytic oxidation rate by the presence of significant water vapor (RH above 50%) (Dibble and Raupp, 1990; Peral and Ollis, 1992; Junio and Raupp, 1993).

Quantitative rate parameters for photocatalytic destruction of acetone at room temperature were extracted from the intrinsic kinetic data of Junio and Raupp (1993). Parameters for isopropyl alcohol (IPA) were similarly extracted from in-house data to be published (Ameen et al., 1997). The kinetics submodel employed provides a good fit to the data over a range of VOC concentrations from 10 to 200 ppm_V, a reasonable fit for RH from 10% to 90%, and a good fit for UV intensities below one UV sun.

The catalyst absorbance A and reflectance R were estimated assuming uniform catalyst coating thickness and no dependence on incidence angle. Optical constant data for dense titania obtained from the literature (Tang et al., 1994a,b) are not consistent with the optical characteristics of the porous thin films employed in this study. Specifically, the absorption coefficient literature value of 28,900 cm^{-1} for anatase thin films is significantly higher than that exhibited by the porous films (Varghese, 1996). We therefore measured transmittance values for the porous films, and used a reflectance value derived from the literature to estimate absorption. To estimate reflectance, the values we employed for the real part of the complex refractive index and the extinction coefficient were 2.5 and 0.0828, respectively (Williams, 1982). The resulting calculated reflectance value of about 18% is slightly lower than measured values reported in the literature, which fall in the range of 20–25% (Tang et al., 1994a,b; Williams, 1982).

Numerical solution of the model equations

The species mass balances can be classified as simultaneous nonlinear ordinary differential equations second order in z and coupled by the reaction rate expression. A central finite difference method using a second-order approximating polynomial was coupled with a globally convergent form of the Newton-Raphson method to solve these equations. The radiation balance equations are also nonlinear ordinary differential equations, but are first-order in r, and are coupled by the forward- and backward-radiation fluxes. A fourth-order Runge-Kutta variable-step-size method was employed to solve these equations.

Experimental Studies

Acetone and IPA conversion data were collected using a bench-scale PCO system, shown in Figure 3. Feed composition and total flow rate can be independently selected by appropriately setting individual flow rates of reactants (organic in N_2, UHP N_2, and air or 1% O_2 in N_2) from pressurized gas cylinders using mass flow controllers (Tylan). Water vapor is added to the feed flow by passing a separate nitrogen flow through a saturator; the degree of saturation is determined by the contact time and the temperature in the saturator. After mixing, the gases are fed to the photoreactor. All reactant lines are heated to a temperature above the source cylinders' and saturator's temperatures to ensure that no condensation takes place within the gas-transport system. The annular photoreactor incorporates a 1.5-in. OD (38-mm-OD) 20-W UV Black Lamp in a 2.25-in. ID (57-mm-ID) glass tube. The annular space is packed with titania-coated quartz beads of 1-mm nominal diameter; bed length is 90 cm. The titania films were prepared with either a washcoat method employing Degussa P25 in a slurry of IPA, or using a modified sol-gel technique employing titanium isopropoxide (Varghese, 1996). In general, thinner, more uniform and better adhering coatings could be achieved with the sol-gel technique. Ultraviolet light fluxes at the lamp and at the reactor outer wall in the range of 300–400-nm wavelength were measured with a Minolta integrating photometer.

The system incorporates three in-line sensors (Sens1, Sens2 and Sens3) and three discrete sampling locations (Sam1, Sam2 and Sam3). Sam1 and Sam2 are automatic multiple-port GC sampling valves (Valco) that send a well-defined volume of gas to one of two columns in the GC for VOC and carbon dioxide analysis, respectively. The third sampling location (Sam3) allows gas samples to be withdrawn for off-line analysis. Sens1 is an in-line relative humidity sensor (Vaisala). Sens2 and Sens3 are in-line electrochemical sensors for HCl and CO measurement, respectively. The feed gases may be analyzed with the sensors and sampling location on the outlet line by bypassing the reactor. Flow-, temperature-, and pressure-measuring devices are also included as indicated in the figure. All measurements are recorded using automatic data acquisition driven by an HP 486 processor-based PC.

The Varian model 3700 gas chromatograph is fitted with both a 6-ft column of 10% SP-2100 on 80/100 Supelcoport

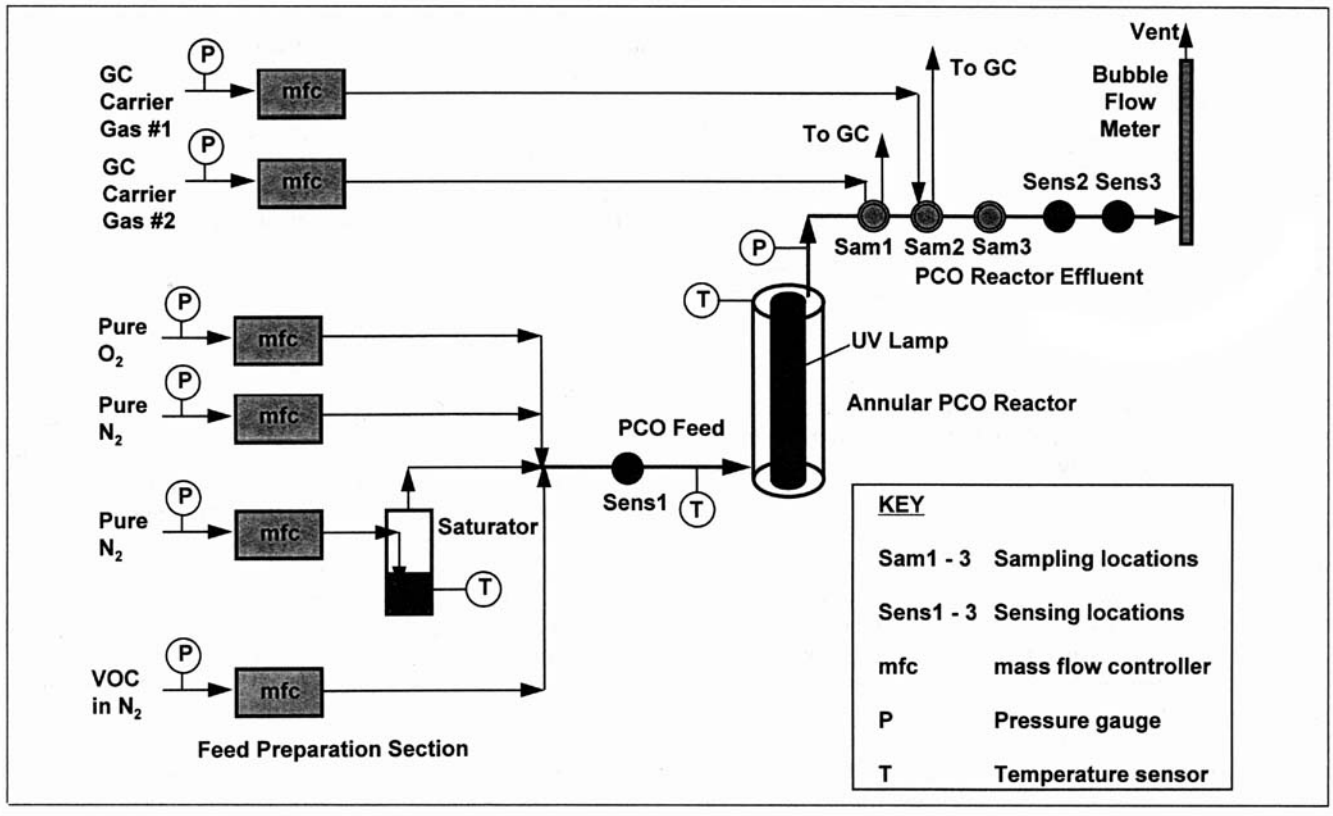

Figure 3. Bench-scale PCO system employed for reactor performance evaluation.

and a 6-ft column of 0.1% SP-1000 on 80/100 Carbopack C equipped with a flame ionization detector (FID). The FID can be used to quantify VOC concentrations from approximately 1 to 10,000 ppm_V. Carbon dioxide analysis is performed with an isothermal mole sieve column and an external methanizer/FID unit (Valco).

Results and Discussion

Figure 4 illustrates the nature of the predictions of the two-flux UV irradiation submodel for 1-mm-diameter spherical catalyst beads coated with a 0.1-μm average thickness sol-gel titania layer. Shown are the dimensionless forward, backward, and total UV flux profiles for the reactor dimensions described earlier. The photon mean free path λ was adjusted to a value of 0.62 mm (62% of the particle diameter) so that the predicted UV flux at the wall ($\xi = 1.0$) matched the average of the measured flux values. This mean free-path value was found to provide a good fit to the wall UV flux values measured for a 2.5-μm wash-coat titania film as well. For the present case where the film is relatively thin, the absorbance is low and significant light transmits all the way through the bed. The gradient is moderate, with the UV flux dropping to about half the source value at half the radial distance through the bed. Recall that a substantial portion of the predicted UV intensity drop is due to a simple geometric $1/r$ factor from the annular configuration.

Figure 5 plots the two-flux submodel-predicted dimensionless UV flux profiles for different titania film thicknesses on 1-mm-diameter spheres. The behavior predicted by the two-flux model mirrors the behavior of the optical properties (A, R, and T) of titania thin films, which vary markedly as film thickness is increased from 0.10 μm to about 5.0 μm. Above this latter thickness the constants change quite gradually with increasing film thickness as asymptotic absorbance values are realized. The two-flux model likewise shows asymptotic behavior in this range of film thickness. For the subject packing configuration, the maximum total light absorption fraction is

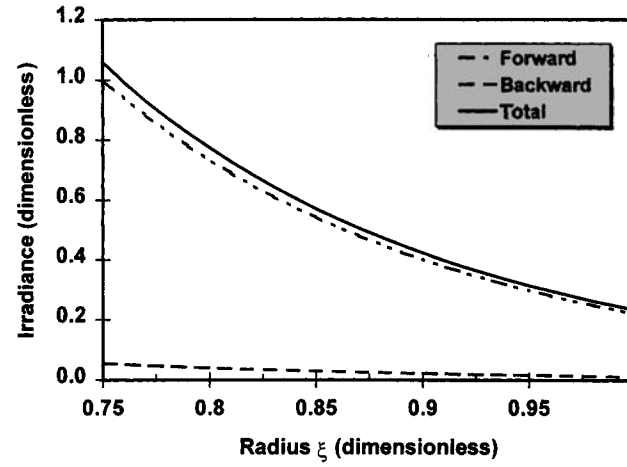

Figure 4. Two-flux model predictions: dimensionless forward, backward, and total UV flux vs. dimensionless annular reactor radial distance for 1-mm-diameter packing coated with a 0.1-μm sol-gel-derived titania film.

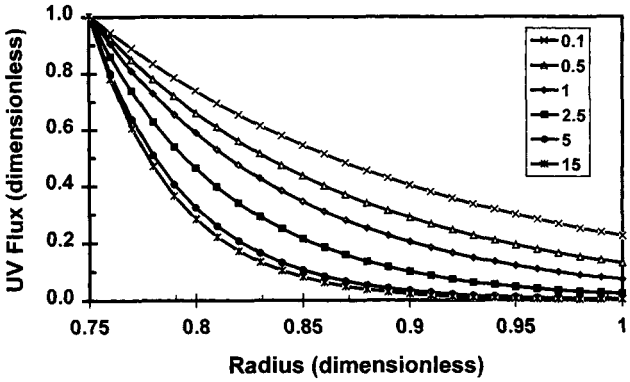

Figure 5. Total UV flux profiles vs. dimensionless annular-reactor radial distance for 1-mm-diameter packing and various titania film thicknesses.

about 0.95, with the maximum occurring at the highest film thickness. For this case, most of the light not absorbed is lost through reflection by catalyst film near the lamp.

The pseudohomogeneous reactor model with the two-flux UV irradiance submodel was used to simulate PCO reactor performance for destruction of 100-ppm$_v$ acetone in humid air. Figure 6 compares model-predicted acetone conversion to experimental data for a range of reactor residence times. In this example, the catalyst film thickness was 2.5 μm. Residence times were estimated from knowledge of the total volumetric flow rate, reactor-bed volume, and void fraction. To obtain a good quantitative agreement between model and experiment, the kinetic parameter Θ_{VOC} was adjusted by approximately 50% from the independently determined value (Junio and Raupp, 1993) so that the conversion at a single data point (0.9 s residence time) matched exactly. This adjusted value was then used in subsequent simulations for the other residence times. With this approach, reasonable agreement between model predictions and experimentally determined acetone conversion is realized. The magnitude of the parameter adjustment necessary to obtain a good quantitative fit to the data is a consequence of the manner in which the independent kinetics were determined. Specifically, kinetic data were collected using a powder-bed reactor (Dibble and Raupp, 1990), in which it was assumed that all light incident on the titania powder was absorbed in the top 15 μm of the bed. The fact that UV reflection was neglected, coupled with the uncertainty in the effective absorption factor for the bed, readily explains the implied uncertainty level in the magnitude of the kinetic parameter.

Even for residence times as high as 2 s, acetone conversion is less than 50%. This limitation reflects both the moderate intrinsic rate of photocatalytic acetone destruction, as well as a suboptimal reactor configuration. This latter issue is explored in greater detail below.

To collect the data summarized in Figure 6, the total contaminated air flow rate was systematically varied with the catalyst bed-length fixed. For these data, the flow characteristics as quantified by the Reynolds number are not constant from data point to data point. Of immediate concern is the potential for gas–solid diffusional mass-transport limitations, as the superficial velocity drops to low values to achieve high residence times. To test the hypothesis that the data were collected in the kinetic control operating regime, the global acetone conversion rate was plotted vs. the square root of the superficial velocity over the diameter of the spherical packing, $(u/d_p)^{1/2}$, as shown in Figure 7. For kinetically controlled data, the global rate is independent of this quantity (Froment and Bischoff, 1990), since the external mass-transfer coefficient is proportional to $(u/d_p)^{1/2}$. The plot reveals that data collected for residence times below around 1.5 s is indeed in the kinetic control regime, although data collected at higher residence times is susceptible to mass-transport limitations. This finding highlights a key concern in practical packed-bed photocatalytic reactor design, since many target VOCs convert at significantly higher intrinsic rates than acetone.

To provide a more rigorous test of the pseudohomogeneous PCO reactor model, the model was used to describe IPA photocatalytic destruction behavior. In IPA conversion, acetone is produced as an undesirable airborne byproduct. Figure 8 compares model predictions to experimental bench-scale data in which the reactor was packed with 1-mm-diameter glass beads and the mean titania film thickness was 2.5 μm. To obtain a good quantitative agreement between model and experiment, the kinetic parameter

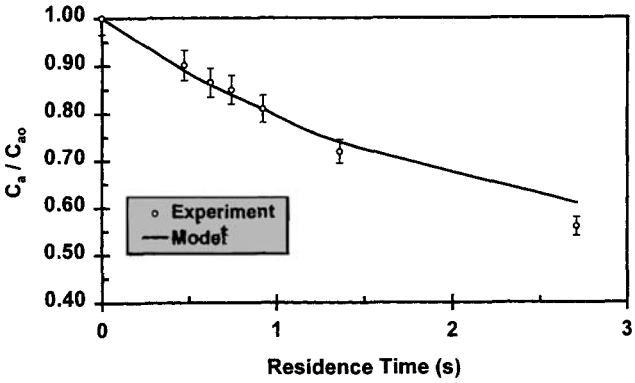

Figure 6. Normalized acetone concentration vs. residence time in an annular packed-bed photocatalytic reactor.

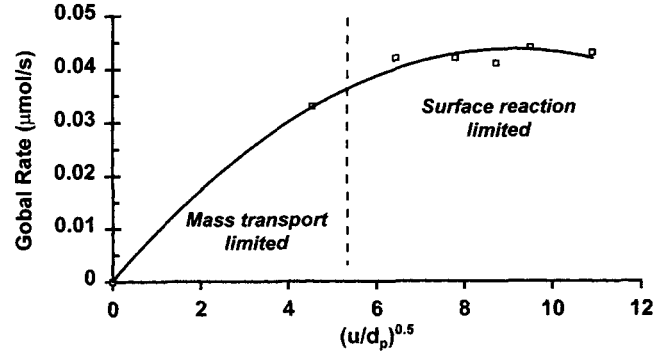

Figure 7. Global acetone conversion rate vs. the square root of the particle diameter over the superficial velocity showing gas–solid diffusional mass-transport-limited and surface-reaction-limited regimes.

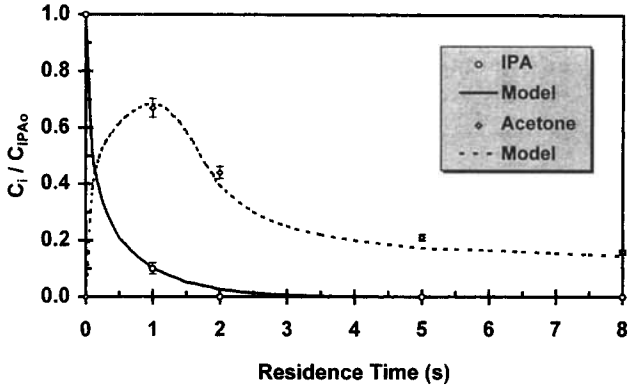

Figure 8. Normalized IPA and acetone concentration vs. residence time in an annular packed-bed photocatalytic reactor.

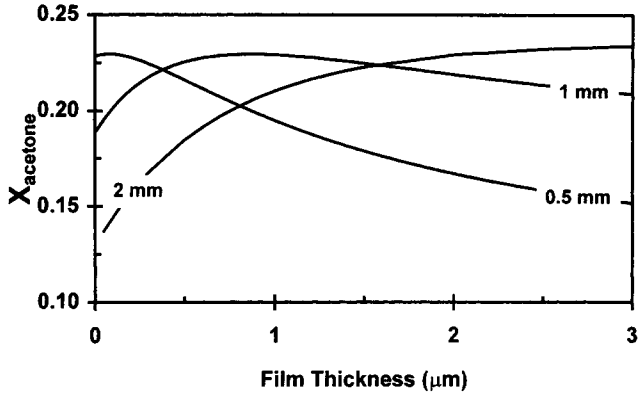

Figure 9. Acetone fractional conversion vs. film thickness for packing diameters of 1, 0.5, and 2 mm; gas residence time fixed at 1 s.

Θ_{VOC} for IPA was adjusted by approximately 30% from the independently determined value (Ameen et al., 1996), so that the IPA conversion at a single data point (1.0-s residence time) matched exactly. Using this approach, the model captures the key experimental features, including the maximum in acetone concentration, reasonably well. The data are characteristic of a consecutive reaction sequence where the rate of destruction of the intermediate is approximately 3–4 times slower than destruction of the parent compound. Because of the disparity in reaction rates, significant acetone destruction to the final carbon dioxide and water-vapor products occurs only after nearly all the IPA is converted.

The validated model can be used with the experimentally extracted parameters to virtually optimize the reactor design through process simulation. Lamp diameters are fixed at discrete values (e.g., 1.5 in. diameter) by the commercial manufacturers. The designer is free to choose the outer reactor-wall diameter (within available standard sizes), as well as the packing material, shape, and size and the photocatalyst mean film thickness. Consider the situation in which reactor wall diameter and packing shape have been chosen, as they have been in this work; variables to be optimized to maximize VOC conversion are then the packing size and photocatalyst film thickness.

Figure 9 illustrates simulations of the acetone conversion vs. titania film thickness for three different packing diameters at a fixed residence time of 1 s. In each case a maximum in conversion is observed, with the location of the maximum strongly dependent on the size of the packing. For the 1-mm-diameter spheres employed in the experiments, the model predicts that the optimum titania film thickness is ca. 0.9 μm. In contrast, the optimum film thickness for 0.5-mm-diameter spheres occurs at 0.1 μm, and the optimum for 2-mm spheres is at approximately 4 μm. The optimum for the 2-mm spheres is quite broad, with film thicknesses from 2 μm to 10 μm, exhibiting nearly equal conversions.

The behavior displayed in Figure 9 can be understood with the aid of Figure 10, which plots the model-predicted LVREA vs. film thickness for the three different packing diameters. Figure 10a shows the profiles for 1-mm-diameter spheres. At low film thickness, the LVREA is reasonably uniform. Conversely, at high film thickness where the film absorbance is high, the LVREA gradient is severe. At the inner region of the annular space the absorbed energy is unnecessarily high, while at the outer region there is almost no light energy absorption. Examination of the details of the reactor model predictions suggests that the performance limitation alluded to earlier is directly related to the reactor configuration. For thick catalyst films, the severe LVREA gradient leads to the buildup of significant radial VOC concentration gradients down the length of the reactor. At the lamp, where the LVREA is high, VOC conversion is likewise high, achieving 100% well before the reactor outlet. Near the reactor wall, however, the LVREA is low since most of the original light emitted from the lamp is absorbed by catalyst in the annular space. This low level of UV energy leads to low reaction rates near the outer wall, and hence low VOC conversion. The bulk concentration at the outlet is the radially averaged concentration, yielding an overall moderate conversion.

For 0.5-mm-diameter beads, shown in Figure 10b, the LVREA gradients are even more severe for a given catalyst thickness. From the viewpoint of the two-flux submodel, the packing number N_p is larger, yielding larger coefficients in the two-flux differential equations, and hence larger UV intensity gradients. Physically, the smaller diameter reduces the photon mean free path, yielding greater possibility for UV photon–catalyst interaction. Hence the optimum catalyst thickness occurs at a significantly lower value than that for the 1-mm-diameter packing. Films thicker than about 1 μm lead to poor utilization of the reactor volume, with a significant fraction of the reactor near the outer wall operating under dark conditions.

If a sufficiently large-size packing is chosen relative to the annular dimensions, then the optimum catalyst thickness is fairly high, corresponding to absorbance greater than 90%. Figure 10c plots the LVREA for such a situation. Here the packing diameter is 2 mm. Because of the limited opportunity for photon–catalyst interaction, even the thickest films yield an LVREA profile that utilizes the reactor volume reasonably well. For no film thickness level does the LVREA drop to negligibly small values, as they do in the previous cases for smaller packing sizes.

The example described earlier for acetone destruction dealt with conversion levels well below unity. In Figure 11, IPA conversion is plotted vs. film thickness for three packing sizes

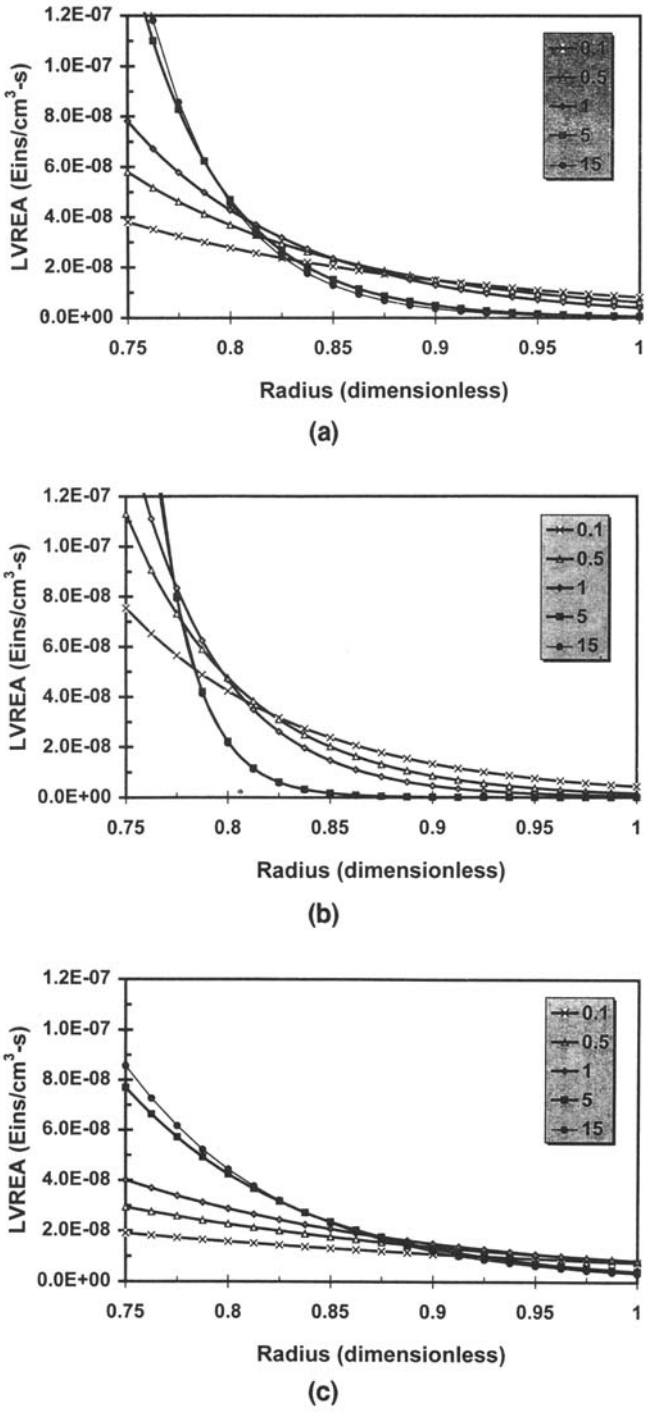

Figure 10. Local volumetric rate of energy absorption (LVREA) vs. dimensionless annular reactor radial distance for various titania film thicknesses.

(a) 1-mm-diameter packing; (b) 1-mm-diameter packing; and (c) 2-mm-diameter packing.

and otherwise fixed conditions that were chosen to yield high conversions. The simulations reveal that conversion can be improved from the 90% value realized for 1-mm-diameter spheres and a 2.5-μm film by reducing the film thickness. For films less than about 1 μm, greater than 99% conversion of

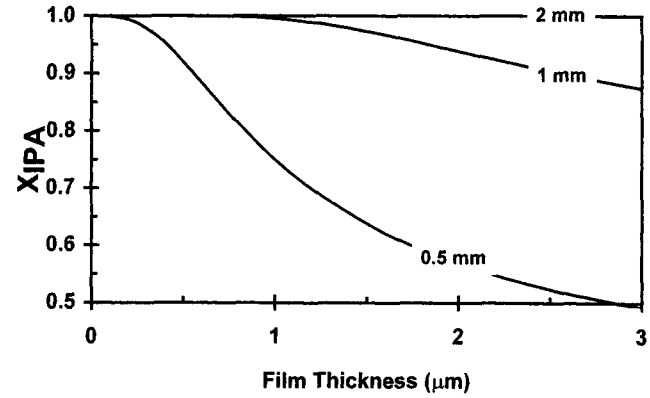

Figure 11. IPA fractional conversion vs. film thickness for packing diameters of 1, 0.5, and 2 mm.

Gas residence time fixed at 1 s.

IPA is predicted. For smaller diameter spheres, the film must be reduced to lower thicknesses, whereas larger diameter spheres allow thicker films to be employed. For example, 0.5-mm-diameter spheres require films thinner than about 0.25 μm, and 2-mm-diameter spheres allows films up to 10 μm to be employed to achieve 99% IPA destruction.

As a final note, recall that the reaction-rate expression employed in this modeling effort assumed a first-order dependence on LVREA. There exists some evidence that, at high UV intensity and hence high LVREA levels, the dependence is better represented by a shifting order, with a limiting half-order dependence at the highest levels. This half-order value is indicative of a photoexcitation–recombination pseudoequilibrium in which relatively few electron-hole pairs participate in PCO reactions, but instead tend to recombine. Such a functionality would tend to further penalize the reactor configurations with high LVREA gradients and shift the film thickness maxima displayed in Figures 9 and 11. This factor highlights the need for valid constitutive relationships in this, as well as any other, quantitative modeling efforts.

Conclusions

A pseudohomogeneous model with a two-flux irradiance submodel was developed to simulate photocatalytic oxidation of dilute VOCs in air in an annular packed-bed reactor. In dimensionless form the two-flux model shows that four dimensionless groups control the magnitude of the UV irradiance profile and the integrated UV absorption in the packed bed. These parameters are directly related to reactor and packing dimensions, catalyst coating thickness, and optical constants. A reasonable agreement was found between model-predicted light flux at the outer reactor wall and experimental values without adjusting any submodel parameters.

The pseudohomogeneous reactor model predictions for acetone conversion agreed well with experimental measurements using a laboratory-scale packed-bed reactor and bench-scale flow and gas analysis system. The model details suggest that the presence of significant radial gradients in UV LVREA leads to significant reaction rate and concentration gradients, which ultimately limit reactor performance.

Based on these promising simulations, we are currently pursuing further model testing and validation work. Once fully validated, this descriptive model can then be used to fully explore the design parameter space to determine the optimal reactor mechanical design and catalyst distribution configuration. Ultimately this work should identify preferred reactor configurations and provide necessary engineering scale-up data for full-scale operation. This information can be used by process development and design engineers to design a full-scale commercial unit and to fully evaluate the economic viability of PCO for practical point-of-use VOC abatement.

Acknowledgments

The authors gratefully acknowledge the Semiconductor Research Corporation, Environmental, Health and Safety Sciences, and the U.S. Environmental Protection Agency, Office of Exploratory Research, for financial support of this work.

Literature Cited

Akehata, T., K. Ito, and A. Inokawa, "Light Intensity Profiles in Bubble-Dispersed Systems," *Kagaku Kougaku Ronbunshu*, **2**, 583 (1976).

Ameen, M., V. A. Burrows, and G. B. Raupp, "Mechanism and Kinetics of the Photocatalytic Oxidation of Isopropanol in Air," *J. Catal.*, (1997).

Dibble, L. A., and G. B. Raupp, "Kinetics of the Gas-Solid Heterogeneous Photocatalytic Oxidation of Trichloroethylene over Near UV-Irradiated Titanium Dioxide," *Catal. Lett.*, **4**, 345 (1990).

Froment, G. F., and K. B. Bischoff, *Chemical Reactor Analysis and Design*, 2nd ed., Wiley, New York, p. 401 (1990).

Formenti, M., F. Juillet, P. Meriadeau, and S. J. Teichner, "Heterogeneous Photocatalysis for Partial Oxidation of Paraffins," *Chem. Technol.*, **1**, 680 (1971).

Gunn, D. L., "Axial and Radial Dispersion in Fixed Beds," *Chem. Eng. Sci.*, **42**, 363 (1987).

Inokawa, A., and T. Akehata, "Light Intensity Profiles in Heterogeneous Annular Photoreactors," *Kagaku Kougaku Ronbunshu*, **6**, 178 (1980).

Junio, C. T., and G. B. Raupp, "Photocatalytic Oxidation of Oxygenated Air Toxics," *Appl. Surf. Sci.*, **72**, 321 (1993).

Maruyama, T., and T. Nishimoto, "Light Intensity Profile in Heterogeneous Photochemical Reactor," *Chem. Eng. Commun.*, **117**, 111 (1992).

Pasquali, M., F. Santarelli, J. Porter, and P.-L. Yue, "Radiative Transfer in Photocatalytic Systems," *AIChE J.*, **42**, 532 (1996).

Peral, J., and D. F. Ollis, "Heterogeneous Photocatalytic Oxidation of Gas-phase Organics for Air Purification: Acetone, 1-Butanol, Butyraldehyde, Formaldehyde, and m-Xylene Oxidation," *J. Catal.*, **136**, 554 (1992).

Sauer, M., "Engineering Aspects of Gas-Solid Photocatalysis: Monolith Configuration, Multiple Reactant Networks, and Catalyst Deactivation," PhD Diss., North Carolina State University, Raleigh (1995).

Spadoni, G., E. Bandini, and F. Santarelli, "Scattering Effects in Photosensitized Reaction," *Chem. Eng. Sci.*, **33**, 517 (1978).

Suzuki, K., "Photocatalytic Air Purification on TiO_2 Coated Honeycomb Support," *Photocatalytic Purification and Treatment of Water and Air*, D. F. Ollis and H. Al-Ekabi, eds., Elsevier, New York, p. 421 (1993).

Tang, H., R. Prasad, R. Sanjines, P. E. Schmid, and F. J. Levy, "Electrical and Optical Properties of Anatase TiO_2," *J. Appl. Phys.*, **75**, 2042 (1994a).

Tang, H., H. Berger, P. E. Schmid, and F. Levy, "Optical Properties of Anatase TiO_2," *Solid State Commun.*, **92**, 267 (1994b).

Turchi, C., National Renewable Energy Laboratory, Golden, CO, personal communication (1995).

Varghese, R., "Preparation and Characterization of Thin Film Photocatalysts for Point-of-Use VOC Abatement," MS Thesis, Arizona State University, Tempe (1996).

Williams, L. M., "Structural and Photoelectrochemical Properties of Plasma Deposited Titanium Dioxide," PhD Diss., University of California, Berkeley (1982).

Wolfram, E., NREL/DOE Subcontractors Meeting, Copper Mountain, CO (1995).

Yokota, T., T. Iwano, and T. Tadaki, "Light Absorption Rate in a Heterogeneous Photochemical Reactor," *Kagaku Kougaku Ronbunshu*, **3**, 248 (1977).

Manuscript received Aug. 7, 1996, and revision received Oct. 1, 1996.